Convective Heat Transfer by Impingement of Circular Liquid Jets

X. Liu
Student Mem. ASME

J. H. Lienhard V
Mem. ASME

J. S. Lombara[1]

Department of Mechanical Engineering,
Massachusetts Institute of Technology,
Cambridge, MA 02139

The impingement of circular, liquid jets provides a convenient method of cooling surfaces. Here, jet impingement cooling of uniformly heated surfaces is investigated analytically and experimentally for stable, unsubmerged, uniform velocity laminar jets in the absence of phase change. Analytical and numerical predictions are developed for a laminar radial film flow. Experiments using undisturbed laminar jets were performed to determine local Nusselt numbers from the stagnation point to radii of up to 40 diameters. Turbulent transition in the film flow is observed experimentally at a certain radius. Beyond this transition radius, a separate turbulent analysis is constructed. Integral method results are compared to numerical results, and Prandtl number effects are investigated. The predictions are found to agree well with the measurements for both laminar and turbulent flow. Predictive formulae are recommended for the entire range of radii.

Introduction

Cooling a surface with an impinging liquid jet is an attractive technique because of its high efficiency and unsophisticated hardware requirements. Applications of jet impingement cooling are varied, and include processing of both metals and molded plastics, cooling of high-efficiency (aircraft) generator coils, and cooling of certain electronic modules. Such jets lend themselves to either convective boiling or to nonevaporative convection, but in both situations the cooling efficiency varies with the radial distance from the point of impact. In this study, we consider the impingement of a circular, unsubmerged, laminar liquid jet on a surface of uniform heat flux. Convective transport, without change of phase, is analyzed theoretically and experimentally, taking account of both the initial laminar flow and the downstream turbulent flow.

An axisymmetric, laminar impinging jet spreads into a thin, laminar liquid film when it impacts a plane surface normal to its axis (Fig. 1). The hydrodynamics of this film have previously been studied theoretically by Watson (1964) and experimentally by Azuma and Hoshino (1984a, 1984b, 1984c, 1984d) and by Olsson and Turkdogan (1966). Watson divided the flow radially into a stagnation region, a boundary layer region with surface velocity equal to jet speed, and a region of viscous similarity with decreasing surface velocity; he noted that the film flow would be terminated by a hydraulic jump at a location independently controlled by downstream conditions. The thickness of the film initially decreases and then increases with radius as viscous wall effects slow the spreading film. Watson employed both viscous similarity and momentum integral solutions.

Watson's theoretical expressions for the laminar boundary layer and similarity region velocity profiles and film thickness were experimentally verified by Azuma and Hoshino (1984b, 1984c) using laser-Doppler measurements. This is in contrast to the results of Olsson and Turkdogan (1966), who measured the surface velocity by dropping bits of cork onto the liquid. Olsson and Turkdogan found poor agreement with Watson's predictions, observing a constant surface velocity lower than the jet speed, and their results have sometimes been used to

deny the presence of a similarity region. However, no conclusive evidence showed that the dropped, buoyant cork actually moved at the liquid surface speed. Since the experimental approach of Azuma and Hoshino is clearly more accurate, we are inclined to give their conclusions greater weight. For the details of Watson's flow field, the reader is referred to his paper. His expressions, and those of a later independent study by Sharan (1984), are quoted hereinafter when needed.

Azuma and Hoshino measured the turbulent transition radius in their system (which used an annular orifice mounted on the plate, rather than an actual impinging jet) and also measured the subsequent velocity profiles. The turbulent film was well characterized by standard boundary layer results, but it did appear to show relaminarization farther downstream as the film slowed and its stability increased.

Using Watson's similarity solution, Chaudhury (1964) analyzed the heat transfer from an isothermal wall in terms of a series solution for the similarity region and an integral solution for the boundary layer region; Carper (1989) has also presented a solution to that problem. Liu and Lienhard (1989) developed predictions of the Nusselt number for uniform heat flux using an integral method and presented limited comparisons to ex-
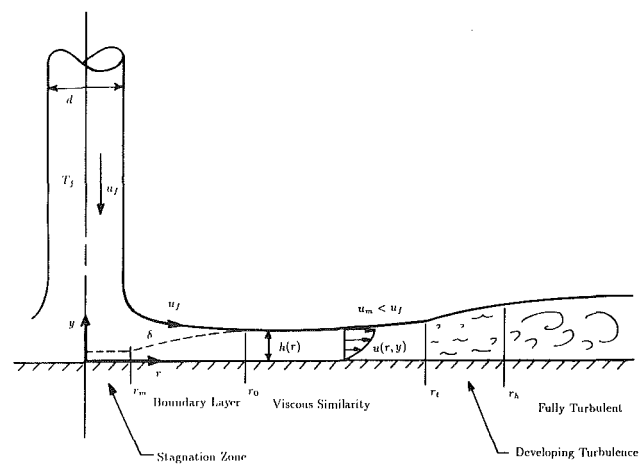

Fig. 1 Jet and film flow field showing hydrodynamic evolution (not to scale)

perimental data. Wang et al. (1989a, 1989b, 1989c) gave detailed theoretical solutions for heat transfer in the stagnation and boundary layer regions; these solutions account for variable wall conditions as well as for conjugate heat transfer between the jet and the wall. They did not consider the downstream similarity region, in which surface velocity declines with radius; at common Reynolds numbers, the stagnation zone and boundary layer regimes are confined to radii of 3 to 7 diameters from the point of impact. When a jet is used to cool large areas, the similarity region and turbulent transition must also be accounted for.

Experimental studies have been few, particularly in regard to local, rather than average, heat transfer. Ishigai et al. (1977) measured local heat transfer coefficients in the hydraulic jump region and presented a limited, graphic set of data for the local heat transfer coefficient in the plane of impact. They mentioned that the data showed a downstream transition from laminar to turbulent flow; their jets were produced by a short tube, three diameters in length. Stevens and Webb (1989) investigated turbulent impinging jet heat transfer experimentally and developed a correlation for Nu_d. Their data are confined to $r/d < 15$ and their correlation is accurate in a region $r/d < 5$ for $d = 2.2$ mm and a smaller region for larger diameter of jets. The radial transition from laminar to turbulent flow was not mentioned, but it must be noted that their jets were deliberately made turbulent prior to impact.

Nakoryakov et al. (1978) used electrodiffusion to obtain local mass transfer coefficients beneath a laminar jet and compared them to an appropriate boundary layer analysis. Their study applies to very high Schmidt number (Sc $\gg$ 1) and a boundary condition of uniform wall concentration, correspondent to uniform wall temperature conditions at Pr $\gg$ 1.

Their experiments showed the mass transfer coefficient to rise above the laminar prediction downstream, and they argued this to result from surface waves. However, the present results suggest that transition to turbulence is a more likely cause in their range of Reynolds number. The incoming jet velocities for their experiments were calculated on the basis of the apparently theoretical stagnation zone result
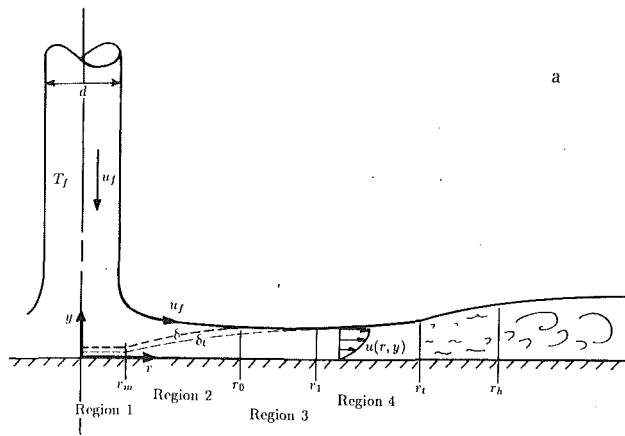
$$Nu_l = 0.753 \, Pr^{1/3} \, Re_l^{1/2} \tag{1}$$

where l is the radius of their electrodiffusion probe. However, this correlation was not independently corroborated in their paper.
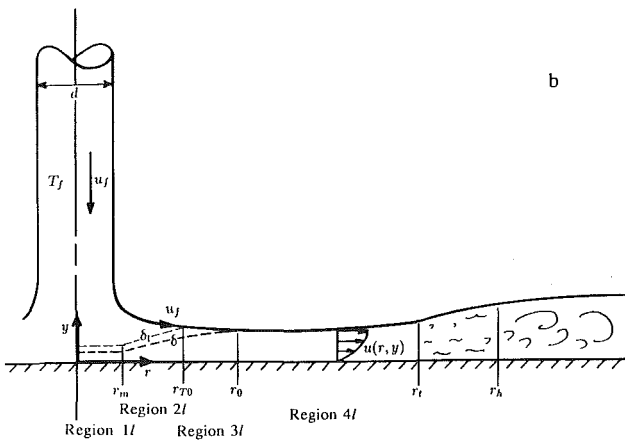
The present paper develops radially complete results for the liquid film heat transfer with uniform heat flux; most of these results are analytically derived, and all are validated experimentally. Particular attention is devoted to the similarity region, employing numerical solutions for the uniform flux condition (which is not self-similar) to investigate the role of wall boundary conditions, simplified correlations, and the integral method prediction of a critical Prandtl number above which the thermal boundary layer does not reach the free surface (Liu and Lienhard, 1989). Our previous integral method solutions are extended to include Pr < 1. The laminar predictions are then compared to new experimental data from an experimental apparatus configured to achieve very clean, stable, laminar jets. The laminar predictions are generally found to agree very well with the data. In addition, turbulent transition is observed in the similarity region, and separate analytical predictions are developed to account for the turbulent augmentation of the heat transfer. A correlation is given for the turbulent transition point.

───────── Nomenclature ─────────────────────

c_p = heat capacity
C_c = jet contraction coefficient = 0.611
C_f = friction factor
d = contracted jet diameter = $\sqrt{C_c} \times$ (diameter of orifice)
$f'(\eta)$ = similarity function, equation (24)
h = local thickness of liquid sheet
h_{r1} = liquid sheet thickness at the position where thermal boundary layer reaches the free surface
h_t = liquid sheet thickness at transition point from laminar to turbulence
h_{T0} = liquid sheet thickness at r_{T0}
k = thermal conductivity of the liquid
k_w = thermal conductivity of the heater
Nu_d = Nusselt number = $q_w d / k(T_w - T_f)$
Nu_r = Nusselt number based on r, = $q_w r / k(T_w - T_f)$ = $Nu_d(r/d)$
Pr = Prandtl number
q_w = wall heat flux
Q = volume flow rate of jet = $u_f \pi d^2 / 4$

r = radius measured from point of jet impact
r_h = hump radius, at which turbulence is fully developed
r_o = radius at which δ reaches the surface of the liquid sheet
r_1 = radius where thermal boundary layer reaches the free surface for Pr > 1
$r_{T,i}$ = location of the initial temperature profile given
r_{T0} = radius where thermal boundary layer reaches the free surface for Pr < 1
$r_{u,i}$ = location of the initial velocity profile given
r_t = radius at transition point from laminar to turbulent flow
R = Reynolds number defined by Watson = $2Q/d\nu$ = $(\pi/2) Re_d$
Re_d = Reynolds number of the jet = $u_f d / \nu$
St = Stanton number = $q_w / \rho c_p u_{max} (T_w - T_{sf})$
t = heater sheet thickness
$T(r, y)$ = liquid temperature distribution
T_f = jet temperature at impingement

T_m = measured temperature on the back of the heater
T_{sf} = free surface temperature
T_{sat} = liquid saturation temperature
T_w = wall temperature on the liquid side of the heater
$u(r, y)$ = radial velocity distribution in liquid film
u_f = velocity of impinging jet
u_{max} = local maximum film velocity (liquid free surface velocity), equal to u_f in regions 2, 2l, and 3l
y = distance normal to the wall
z = distance between nozzle and target plate
δ = viscous boundary layer thickness
δ_t = thermal boundary layer thickness
Δ = δ/h
Δ_{T0} = Δ at r_{T0}
ϵ = (t/d);ϵ^2 is the order of radial to vertical conduction in the heater sheet
η = similarity variable
θ = nondimensional temperature
μ = dynamic viscosity
ν = kinematic viscosity
ρ = density
ϕ = δ/δ_t

Fig. 2 Development of the thermal boundary layer: (a) Pr > 1; (b) Pr < 1 (not to scale)

2 Predictions From the Laminar Theory

2.1 Integral Solutions for the Heat Transfer: Pr ≥ 1. In a previous study (Liu and Lienhard, 1989), we obtained integral solutions for the heat transfer in the boundary layer and similarity regions for Prandtl number greater than the unity. The regions identified and results found are as follow (see Fig. 2a):

Region 1. The stagnation zone.
Region 2. $\delta < h$ *region:* Neither the thermal nor viscous boundary layer reach the free surface; surface temperature and velocity, T_{sf} and u_{max}, are the inlet temperature and velocity, T_f and u_f.
Region 3. $\delta = h$ *and* $\delta_t < h$ *region:* The viscous boundary layer has reached the free surface. The velocity outside the viscous boundary layer decreases with radius, but the surface temperature remains at the inlet temperature, T_f.
Region 4. $\delta = h$, $\delta_t = h$, *and* $T_w < T_{sat}$ *region:* In this region, the thermal boundary layer has reached the surface of the liquid sheet, and the temperature of the liquid surface increases with radius.
For region 2, the boundary layer region follows the stagnation zone:

$$\mathrm{Nu}_d = 0.632 \, \mathrm{Re}_d^{1/2} \, \mathrm{Pr}^{1/3} \left(\frac{d}{r}\right)^{1/2} \qquad (2)$$

Region 2 ends and region 3 begins where the viscous boundary layer reaches the film surface at $r = r_0 = 0.1773d \, \mathrm{Re}_d^{1/3}$. In region 3:

$$\mathrm{Nu}_d = \frac{0.407 \, \mathrm{Re}_d^{1/3} \, \mathrm{Pr}^{1/3} \left(\frac{d}{r}\right)^{2/3}}{\left[0.1713\left(\frac{d}{r}\right)^2 + \frac{5.147r}{\mathrm{Re}_d d}\right]^{2/3} \left[\frac{1}{2}\left(\frac{r}{d}\right)^2 + C_3\right]^{1/3}} \qquad (3)$$

where[2]

$$C_3 = \frac{0.267(d/r_0)^{1/2}}{\left[0.1713\left(\frac{d}{r_0}\right)^2 + \frac{5.147_{r_0}}{\mathrm{Re}_d d}\right]^2} - \frac{1}{2}\left(\frac{r_0}{d}\right)^2 \qquad (4)$$

Region 3 ends and region 4 begins where the thermal boundary layer reaches the liquid surface at $r = r_1$; equations defining r_1 are given in our previous paper. In region 4:

$$\mathrm{Nu}_d = \frac{0.25}{\frac{1}{\mathrm{PrRe}_d}\left(1 - \frac{r_1^2}{r^2}\right)\left(\frac{r}{d}\right)^2 + 0.130\frac{h}{d} + 0.0371\frac{h_{r1}}{d}} \qquad (5)$$

where h is given by equation (20) below. Note that region 4 will occur only for Pr less than a critical value near five[3]; otherwise, the thermal boundary layer does not grow fast enough to reach the surface of the liquid film, which thickens at increasing radius owing to viscous retardation. This Prandtl number prediction is of particular interest, and we shall explore it further using numerical solutions for the viscous flow regime below. Regions 3 and 4 correspond to Watson's self-similar viscous flow regime.

2.2 Integral Solutions for the Heat Transfer: Pr < 1. As noted in our previous paper, the region map changes for small Prandtl number (see Fig. 2b):

Region 1l. The stagnation zone.
Region 2l. $\delta_t < h$ *region:* Neither the thermal nor viscous boundary layer reaches the free surface; surface temperature and velocity, T_{sf} and u_{max}, are the inlet temperature and velocity, T_f and u_f.
Region 3l. $\delta_t = h$ *and* $\delta < h$ *region:* The thermal boundary layer has reached the free surface. The surface temperature increases with radius, but the velocity outside the viscous boundary layer is still the jet velocity, u_f.
Region 4l. $\delta = h$, $\delta_t = h$, *and* $T_w < R_{sat}$ *region:* In this region, the viscous boundary layer has reached the surface of the liquid sheet, and the velocity of the liquid surface decreases with radius.

The integral energy equation may be used to estimate the Nusselt number:

$$\frac{d}{dr}\int_0^{\delta_t} ru(T - T_f)dy = \frac{q_w}{pc_p}r \qquad (6)$$

In region 2l, we approximate the velocity and temperature profiles as

$$T - T_w = (T_f - T_w)\left[\frac{3}{2}\frac{y}{\delta_t} - \frac{1}{2}\left(\frac{y}{\delta_t}\right)^3\right] \qquad (7)$$

$$u = u_{max}\left[\frac{3}{2}\frac{y}{\delta} - \frac{1}{2}\left(\frac{y}{\delta}\right)^3\right] \qquad y < \delta$$
$$= u_f \qquad y \geq \delta \qquad (8)$$

These profiles satisfy no slip at the wall, have no shear or heat flux at the free surface (i.e., negligible evaporation; Liu and Lienhard, 1989), and match the local wall temperature. Integration of equation (6) with these profiles yields

---

[2] We have here corrected a minor typographical error in the expression for C_3 appearing in our previous paper.
[3] Our previous paper gave this value as 4.86. If the higher-order terms in the integral analysis are retained, the value becomes 5.23, which is 7 percent higher than the previous one.

$$\mathrm{Nu}_d = \left[\frac{\frac{9}{16}\mathrm{Re}_d\mathrm{Pr}\left(\frac{r}{d}\right)\left(1-\phi+\frac{2}{5}\phi^2-\frac{1}{35}\phi^4\right)}{\frac{1}{2}\left(\frac{r}{d}\right)^2+C} \right]^{1/2} \quad (9)$$

$$\phi = \frac{\delta}{\delta_t} = 1.786\,\mathrm{Nu}_d\left(\frac{r}{d\mathrm{Re}_d}\right)^{1/2} \quad (10)$$

and C is a constant used to match to the stagnation zone. (The stagnation zone is discussed in Section 4.4 below.) If we assume that at the match point r_m, $\mathrm{Nu}_d = \mathrm{Nu}_{d,m}$ and $\phi = \phi_m$, then

$$C = \frac{9}{16}\frac{\mathrm{Re}_d\mathrm{Pr}}{\mathrm{Nu}_{d,m}^2}\left(\frac{r_m}{d}\right)\left(1-\phi_m+\frac{2}{5}\phi_m^2-\frac{1}{35}\phi^4\right) - \frac{1}{2}\left(\frac{r_m}{d}\right)^2 \quad (11)$$

If δ/δ_t is very small and C is also negligible (as shown in section 4), equation (11) can be further simplified to

$$\mathrm{Nu}_d = 1.06\,\mathrm{Re}_d^{1/2}\mathrm{Pr}^{1/2}\left(\frac{d}{r}\right)^{1/2} \quad (12)$$

Region $2l$ ends where the thermal boundary layer reaches the surface of the liquid sheet at $r = r_{T0}$:

$$\frac{r_{T0}}{d} = \frac{0.1984\mathrm{Re}_d^{1/3}\mathrm{Pr}^{1/3}}{\left(1-0.7107\mathrm{Pr}^{1/2}\right)^{2/3}} \quad (13)$$

In region $3l$, $\delta_t = h$ and the temperature of the liquid surface, T_{sf}, is an increasing function of r. The temperature profile in this region is

$$T - T_w = (T_{sf} - T_w)\left[\frac{3}{2}\frac{y}{h}-\frac{1}{2}\left(\frac{y}{h}\right)^3\right] \quad (14)$$

At r_{T0}, the beginning of region $3l$, $\mathrm{Nu}_d = \mathrm{Nu}_{d,T0}$, $h = h_{T0}$, and $\delta = \delta_{T0}$, where h and δ can be computed from Sharan's equations (1984):

$$\frac{h}{d} = 0.125\left(\frac{d}{r}\right)+1.005\left(\frac{r}{\mathrm{Re}_d d}\right)^{1/2} \quad (15)$$

$$\frac{\delta}{d} = 2.679\left(\frac{r}{\mathrm{Re}_d d}\right)^{1/2} \quad (16)$$

Integration of equation (6) from $r = r_{T0}$ with equations (8) and (14) gives

$$\left(\frac{\mathrm{Nu}_d}{2(1-\frac{3}{8}\Delta)}\right)^{-1} = \frac{r}{\mathrm{Re}_d\mathrm{Pr}h}\left(1-\left(\frac{r_{T0}}{r}\right)^2\right)$$
$$+\frac{4}{3}\frac{h}{d}\left(\frac{5}{8}-\frac{3}{20}\Delta^2+\frac{3}{280}\Delta^4\right)-\frac{4}{3}\frac{h_{T0}}{d}\left(\frac{5}{8}-\frac{3}{20}\Delta_{T0}^2+\frac{3}{280}\Delta_{T0}^4\right)$$
$$+2\frac{r_{T0}h_{T0}}{rh}\left(1-\frac{3}{8}\Delta_{T0}\right)\frac{1}{\mathrm{Nu}_{T0}} \quad (17)$$

where $\Delta = \delta/h$. If the terms in Δ are neglected, this simplifies to
Nu_d

$$= \frac{2}{\frac{r}{\mathrm{Re}_d\mathrm{Pr}h}\left(1-\left(\frac{r_{T0}}{r}\right)^2\right)+0.833\frac{h}{d}-0.833\frac{h_{T0}}{d}+2\frac{r_{T0}h_{T0}}{rh}\frac{1}{\mathrm{Nu}_{T0}}} \quad (18)$$

Region $4l$ begins at $r_0 = 0.1773\,d\mathrm{Re}_d^{1/3}$, where the viscous boundary layer reaches the surface; here, the surface velocity decreases with radius. Sharan's integral analysis (1984) shows that

$$u_{max} = \frac{1}{5}\frac{u_f d^2}{hr} \quad (19)$$

where

$$h = 0.1713\left(\frac{d^2}{r}\right)+\frac{5.147}{\mathrm{Re}_d}\left(\frac{r^2}{d}\right) \quad (20)$$

(Equation (20) is in good agreement with Watson's expression for h, which is based on velocity profile of the similarity solution.) The velocity profile is equation (8) with $\delta = h$ and u_{max} from equation (19), while the temperature profile is still equation (14). At $r = r_0$, $h = h_0$ and $\mathrm{Nu}_d = \mathrm{Nu}_{d,0}$. Integration of equation (6) from $r = r_0$ yields

$$\mathrm{Nu}_d = \frac{0.25}{\frac{1}{\mathrm{Re}_d\mathrm{Pr}}\left(\frac{r^2}{d^2}-\frac{r_0^2}{d^2}\right)+0.130\left(\frac{h_0}{d}-\frac{h}{d}\right)+0.25\frac{1}{\mathrm{Nu}_{d,0}}} \quad (21)$$

2.3 Numerical Integration in the Viscous Similarity Region. In the region of viscous similarity, we may solve the nonsimilar boundary-layer energy equation numerically in order to evaluate the accuracy of the integral method solutions for regions 3 and 4 (Pr > 1) and for region $4l$ (Pr < 1). In addition, we may probe the predicted critical Prandtl number for the occurrence of region 4 and the general differences between regions 3 and 4.

Chaudhury (1964) used Watson's velocity similarity to transform the energy equation in the film into the following form:

$$\frac{\partial^2 T}{\partial \eta^2} = \mathrm{Pr}f'\frac{(r^3+l^3)}{r^2}\frac{\partial T}{\partial r} \quad (22)$$

Here, the velocity similarity profile is (Watson, 1964)

$$\frac{2}{c^2}f'(\eta) = \sqrt{3}+1-\frac{2\sqrt{3}}{1+cn[3^{1/4}c(1-\eta)]} \quad (23)$$

where cn is a Jacobi elliptic function, $c = 1.402$, the similarity coordinate is

$$\eta = \frac{y}{h} = \frac{3\sqrt{3}Qr}{2\pi^2\nu(r^3+l^3)}y \quad (24)$$

and the length l is

$$l = 0.3243d\,\mathrm{Re}_d^{1/3} \quad (25)$$

We may nondimensionalize r and l in equation (22) with r_0, the radius at which the viscous boundary layer reaches the liquid surface ($0.1833d\,\mathrm{Re}_d^{1/3}$, according to Watson's analysis[4]). Temperature is nondimensionalized as

$$\theta = \frac{T-T_f}{\Delta T} \quad (26)$$

where ΔT is chosen for convenience as $\Delta T = (2\pi^2\nu q_w r_0^2)/(3\sqrt{3}kQ)$ for uniform wall heat flux and as $\Delta T = T_w - T_f$ for uniform wall temperature. The differential equation is then

$$\frac{\partial^2\theta}{\partial\eta^2} = \mathrm{Pr}f'(\eta)\frac{\bar{r}^3+\bar{l}^3}{\bar{r}^2}\frac{\partial\theta}{\partial\bar{r}} \quad (27)$$

The thermal boundary condition at the wall is

$$\frac{\partial\theta}{\partial\eta}\bigg|_{\eta=0} = -\frac{\bar{r}^3+\bar{l}^3}{\bar{r}} \quad (28)$$

for uniform flux and

$$\theta|_{\eta=0} = 1 \quad (29)$$

for uniform temperature. The free surface is assumed to experience negligible evaporation or convection, so that

[4]Watson found a Blasius velocity profile upstream of the similarity region. The integral method's algebraic velocity profile gives a constant of 0.1773, rather than 0.1833 (3.4 percent lower). To maintain consistency within each approach, we apply 0.1773 with our integral solutions and 0.1833 with the differential equation solutions.
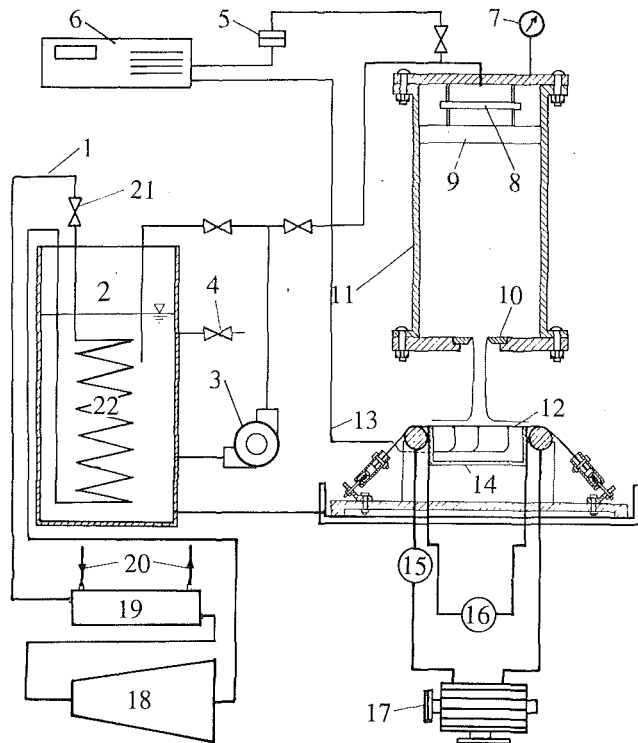
Fig. 3 Experimental apparatus: 1. Freon line; 2. chilled water tank; 3. pump; 4. water supply line; 5. pressure transducer; 6. digital voltmeter; 7. pressure gage; 8. momentum dissipating plate; 9. honeycomb; 10. sharp-edged orifice plate; 11. plenum; 12. steel heater sheet; 13. thermocouple leads; 14. pressurized plastic box; 15. ammeter; 16. voltmeter; 17. 30 kW generator; 18. compressor; 19. heat exchanger; 20. cooling water; 21. throttling valve; 22. evaporator

$$\frac{\partial \theta}{\partial \eta}\bigg|_{\eta=1} = 0 \qquad (30)$$

This approximation is valid for low liquid surface temperatures (Liu and Lienhard, 1989).

The numerical integration begins at $\bar{r} = 1$ $(r = r_0)$. The temperature profile at this station is the initial condition for the solution; tests (see below) show that the initial profile is quickly damped and has little influence on the Nusselt number downstream. The following initial profile was employed:

$$\frac{T - T_f}{T_w - T_f} = 1 - \frac{3y}{2\delta_t} + \frac{1}{2}\left(\frac{y}{\delta_t}\right)^3 \qquad y \le \delta_t \qquad (31)$$

$$= 0 \qquad \delta_t \le y \le \delta \qquad (32)$$

which again satisfies the boundary conditions (no surface flux and matching to T_w). The wall temperature and boundary layer thickness were selected to match those of the upstream boundary layer as calculated from the integral solution. The differential equation was integrated using the Crank–Nicholson procedure.

3 Experiments

Experiments were performed to determine the wall temperature distribution and Nusselt number that actually occur in jet impingement cooling. The experimental arrangement is shown in Fig. 3. The apparatus is in three primary parts: a water jet loop, a refrigerating system, and an electrical heating system.

In our previous paper, the experimental jets showed significant disturbances and sometimes splattered. To prevent splattering, a new apparatus was built specifically to produce uniform velocity-profile, laminar jets free of the surface disturbances that produce splattering (Vasista, 1989). A large plenum with an inlet momentum-breakup plate and turbulence dissipating honeycomb was used to create a pressurized liquid supply free of disturbances from the incoming flow. The jets studied were produced at the bottom of the plenum. The stability of liquid jets is very sensitive to the type of nozzle producing the jet. Pipelike nozzles provide turbulent liquid to the jet when the Reynolds number exceeds a relatively small value (2000–4000); this turbulence generally leads to disturbances in the liquid surface, which are unstable and which are strongly amplified when the jet impacts a flat surface (Errico, 1986). In the present experiments, carefully machined sharp-edged orifice plates were used, rather than pipelike nozzles. Sharp-edged orifices yield laminar, undisturbed jets of high stability. Thus, splattering was entirely suppressed in the present experiments.

The liquid supply was chilled by a mechanical refrigerator before being pumped to the plenum. The water was cooled to near 4°C. This cooling served two purposes. The first was to ensure that the liquid free-surface temperature would not become high enough to produce significant evaporative heat loss at any point along the heater surface (Liu and Lienhard, 1989). The second was to increase the accuracy of the experiments: The requirement of low evaporative loss necessitates relatively low heat fluxes and consequently small differences between wall and inlet temperatures. Subcooling the liquid supply maximized the measured ΔT, without creating evaporative loss, and thus decreased the uncertainty in the measured Nusselt number.

The liquid jets impinge on a heater made of 0.10-mm-thick, 15.2-cm-wide stainless steel sheet. The sheet is stretched over the open top of a 15.2 cm by 17.7 cm plexiglass insulation box and over 2.54-cm-dia. copper rods, which serve as electrodes; springs maintain the tension in the sheet as it expands thermally and prevent its vibration or deflection. The insulation box keeps water away from the underside of the heater sheet, and restricts underside heat losses to a negligible natural convection loss. The box is slightly pressurized with compressed air to prevent liquid inflow. A 15 V, 1200 amp generator powers the sheet directly; the generator was run at up to 20 percent of full power.

The wall temperature distribution is measured by 0.076 mm J-type thermocouples attached to the underside of the sheet and electrically insulated from it by high-temperature Kapton tape. Starting at the stagnation point of the jet, the thermocouples are placed at radial increments of 1.27 cm along the arcs of circle centered at the stagnation point, within a sector of very small angle. The azimuthal symmetry of the flow is very high, and the mechanical convenience of this arrangement was found to introduce no error.

Radial conduction in the heater sheet may be shown to be of order $\epsilon^2 = (t/l)^2$ relative to vertical conduction, where l is the length scale associated with radial changes in the heat transfer coefficient. For the jets, l is essentially the jet diameter, d, so that $\epsilon^2 \approx 0.001$. Radial conduction is thus negligible in comparison to vertical conduction; a formal perturbation solution of the heat equation substantiates this conclusion.

Convective backloss, via natural convection below the heater, is likewise negligible relative to the convective cooling at the upper surface of the heater; the back is essentially adiabatic. At the stagnation point, backloss is less than 0.2 percent of the total flux, owing to the very high liquid-side Nusselt number. The backloss increases downstream, as the Nusselt number declines, but even in the worst case, at the largest radius, this loss is less than 4 percent. Because the backloss is so small, the temperature drop through the 0.06 mm thick Kapton tape (which electrically isolates the thermocouples) was entirely negligible and required no temperature correction.

The vertical conductive temperature drop through the electrical heater, however, can be appreciable in regions where the surface heat transfer coefficient becomes large, principally the stagnation zone. Solution of the heat equation, through terms
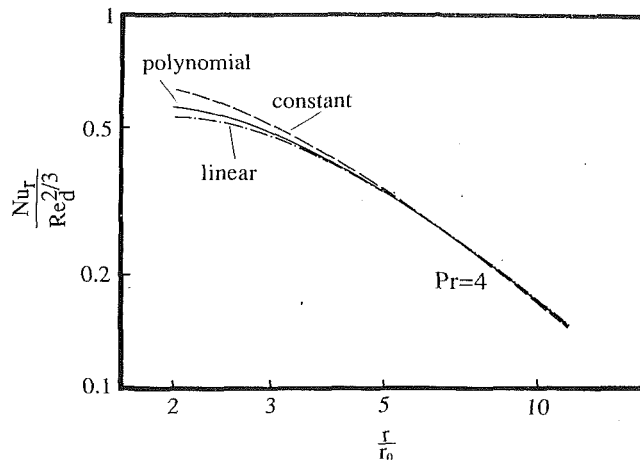
Fig. 4 Effect of initial conditions on the solution of the differential equations in the viscous similarity region for Pr = 4
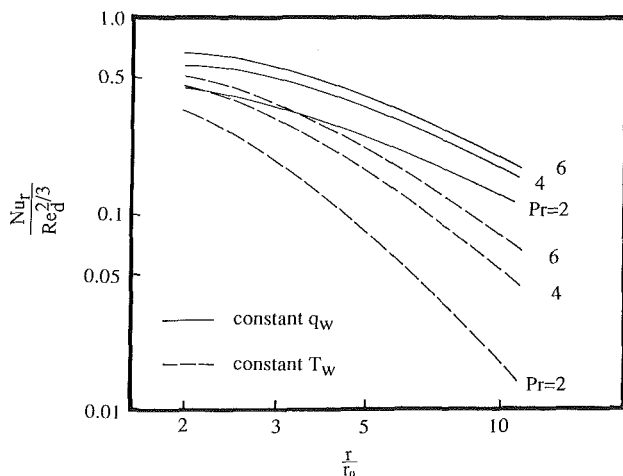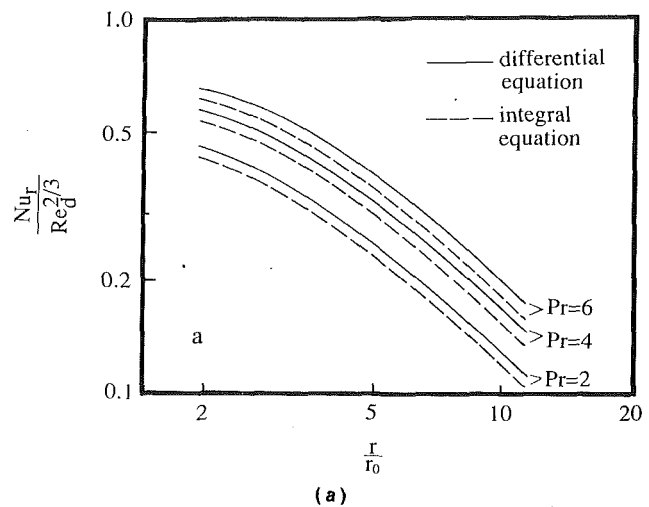

(a)

Fig. 5 Comparison of uniform heat flux and uniform temperature wall conditions in the viscous similarity region (from differential equation)
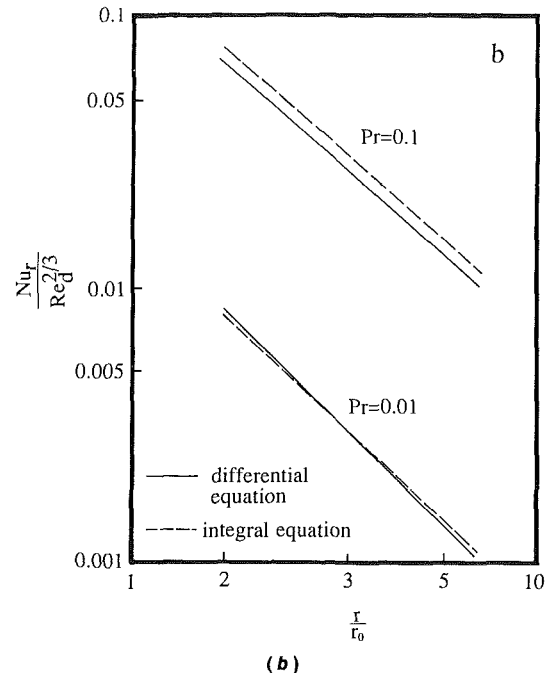

(b)

Fig. 6 Comparison of the solutions from differential and integral analysis of the viscous similarity region at $Re_d = 10^4$ for: (a) Pr > 1; and (b) Pr < 1

of order $\epsilon = t/d$, shows that the ratio of the true Nusselt number, based on liquid-side temperature ($Nu_t = q_w d/k(T_w - T_f)$) to the measured Nusselt number, based on temperature at the back of the heater ($Nu_m = q_w d/k(T_m - T_f)$) is

$$\frac{Nu_t}{Nu_m} = \frac{1}{1 - \zeta Nu_m/2} \quad (33)$$

where $\zeta = tk/k_w d$ relates the Biot number to the true Nusselt number. This temperature correction was applied in reducing the measured data. For the majority of our measurements, the correction is less than 10 percent of the Nusselt number. However, in the stagnation region, particularly when using the smallest orifice (3.18 mm), the correction could be as large as 30 percent.

For each thermocouple measurement, a number of values were taken to reduce random error. These measured values were averaged to get the actual values for the calculations. The thermocouples were also calibrated under isothermal conditions before and after each run to reduce systematic errors. The wall temperature increases with radius and the local Nusselt number is based on the temperature differences between the wall and the incoming jets. At the stagnation point, the temperature differences are smallest and the uncertainty is largest. For 3/8 in. (9.5 mm) diameter orifice it is ±30 percent. The uncertainty goes down very rapidly as radius increases and for most positions uncertainty is less than ±5 percent. Further reduction of stagnation zone uncertainty, by increasing the heat flux, was untenable as a result of the requirement of minimizing downstream evaporation. The uncertainty for Re_d is less than ±2 percent and that for r is less than ±0.25 mm.

Discussion

4.1 Comparison of Integral and Differential Solutions. Numerical integration of the differential equation (22) requires the temperature distribution at the beginning of the similarity region. The exact temperature distribution depends on the upstream stagnation and boundary layer regions. In our calculations, that distribution is based on the polynomial solution from the integral method. However, to test the effects of this initial condition, the computation was also run with an initially linear temperature distribution, between T_w and T_f, in the boundary layer and with a uniform initial temperature, at T_f. The bulk temperatures of these two profiles are larger and smaller, respectively, than that of the polynomial, while the initial slopes of the profiles near the wall are smaller and larger, respectively. Thus, the linear profile gives a lower initial Nu_d and the uniform profile gives a higher initial Nu_d. Figure 4 compares the computations for the different initial temperature profiles. By $r/r_0 = 3$, the difference between the linear, polynomial, and constant initial temperature profiles has decreased to less than 10 percent, and the profiles are indistin-
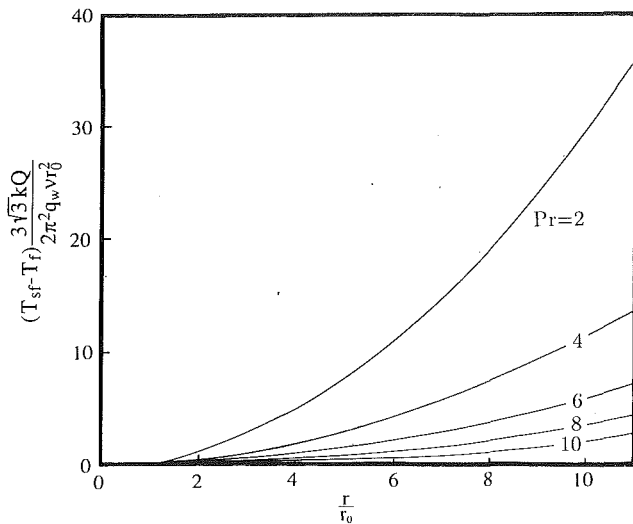
Fig. 7 Effect of Prandtl number on the free surface temperature in the viscous similarity region (from differential equation)
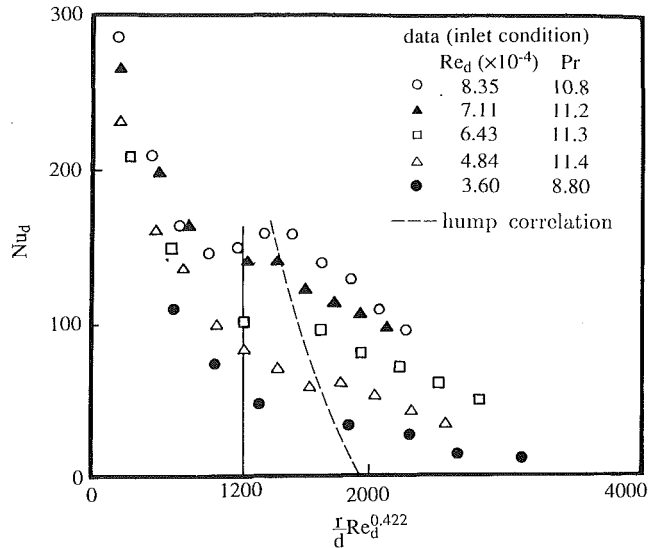
$(T_{sf}-T_f)\dfrac{3\sqrt{3}kQ}{2\pi^2 q_w \nu r_0^2}$ vs $\dfrac{r}{r_0}$

Fig. 9 Turbulent transition as manifested in the Nusselt number

data (inlet condition)

	$Re_d (\times 10^{-4})$	Pr
○	8.35	10.8
▲	7.11	11.2
□	6.43	11.3
△	4.84	11.4
●	3.60	8.80

–––– hump correlation

$\dfrac{r}{d}Re_d^{0.422}$

○ present data

–––– present correlation

– – – Azuma & Hoshino's correlation

$\dfrac{r_t}{d}$ vs $\dfrac{2Q}{d\nu}=\dfrac{\pi}{2}Re_d$
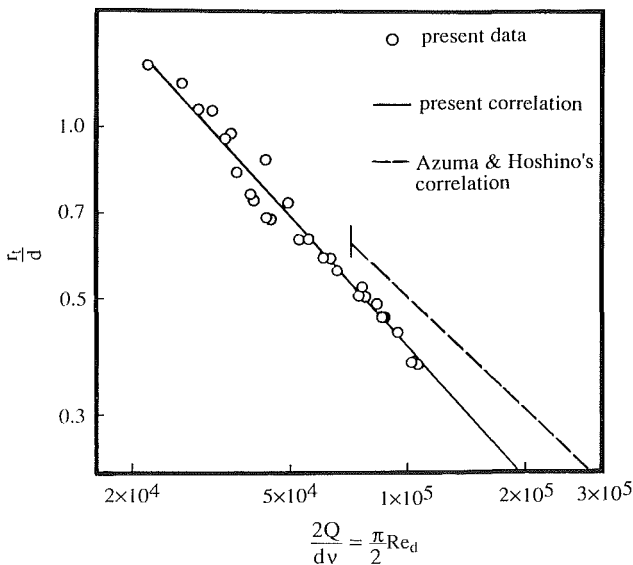
Fig. 8 Radii for transition from laminar to turbulent flow

○ hump data

– – – hump correlation

––––– transition correlation $(\dfrac{r_t}{d})$

Re_d

Fig. 10 Transition and hump radii

guishable at larger r/r_0. Thus, the initial temperature distribution has minimal influence on the Nusselt number in the region far from the center, and results based on the polynomial initial distribution are clearly satisfactory. Moreover, these tests show that the heat transfer in the stagnation zone and boundary layer regimes have little effect on the wall temperature at large radii.

Figure 5 compares heat transfer coefficients for uniform wall heat flux (UHF) to those for uniform wall temperature (UWT) from the differential equation solution. In our previous paper, we noted that, in the boundary layer region, the heat transfer coefficient for UHF was 25 percent higher than that for UWT. By contrast, in the similarity region, the difference between boundary conditions increases with increasing radius. Once the thermal boundary layer reaches the free surface, the energy from the wall is absorbed by the entire film, a situation comparable to fully developed duct flow. However, the UHF condition for the radial film differs markedly from the duct flow, in that the heat transfer surface increases linearly with radius. The UHF condition of the jet is akin to a duct flow with flux increasing linearly with axial position, and such a condition is known to produce a higher heat transfer coeffi-
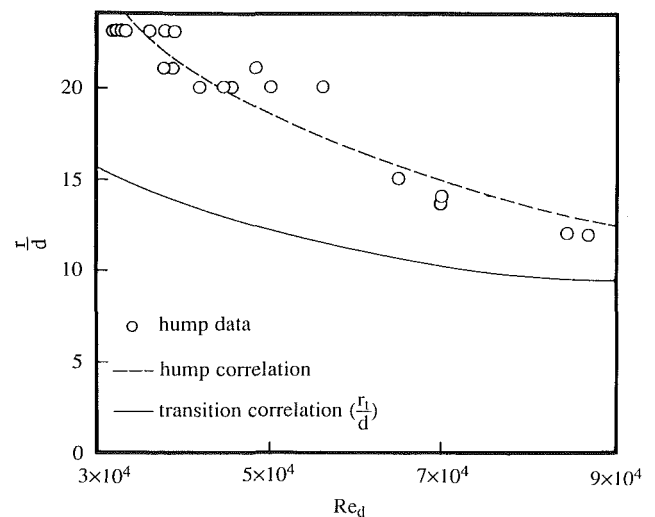
cient. This conclusion is not altered by our definition of Nu_d in terms of incoming, rather than bulk, temperature.

The figure shows that, for small Prandtl numbers, the UWT Nusselt number decreases more rapidly than for large Prandtl number, since the driving temperature difference between wall and surface temperature dwindles much faster at low Pr. At $r/r_0 = 10$, the UWT Nusselt number for Pr $= 2$ is only 9 percent as large as that UHF, and that for Pr $= 6$ is only 40 percent.

Nusselt numbers from the integral and differential equations are compared in Figs. 6(a, b) for Pr > 1 and Pr < 1, respectively.[5] For Pr > 1, the maximum difference between the integral and differential solutions is about 10 percent. The integral solution is lower than the differential equation solution as a result of the assumed shape of the temperature distribution. The integral solution neglects the higher order terms in δ_t/δ, which should cause more error as Pr decreases toward unity, but the comparison shows better agreement with the differential equation solution at lower Pr. Apparently, the neglect of higher order terms compensates for the somewhat smoother profile of the integral procedure. For Pr < 1, Fig.

––––––––––
[5]The ordinate $Nu_r/Re_d^{2/3}$ follows naturally from the scaling of the differential equation, but does not carry the full dependence on Re_d.
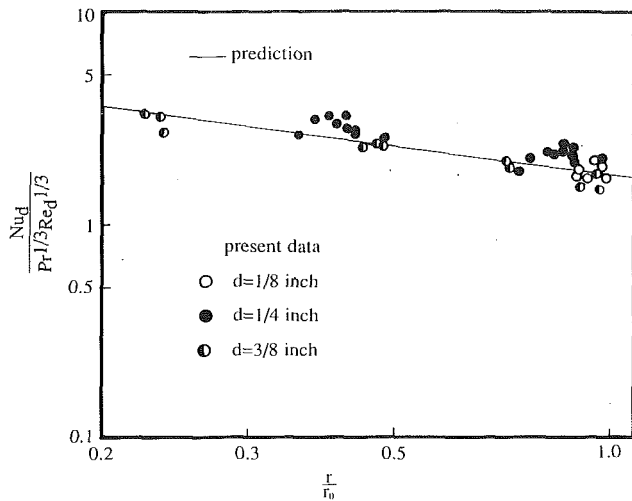
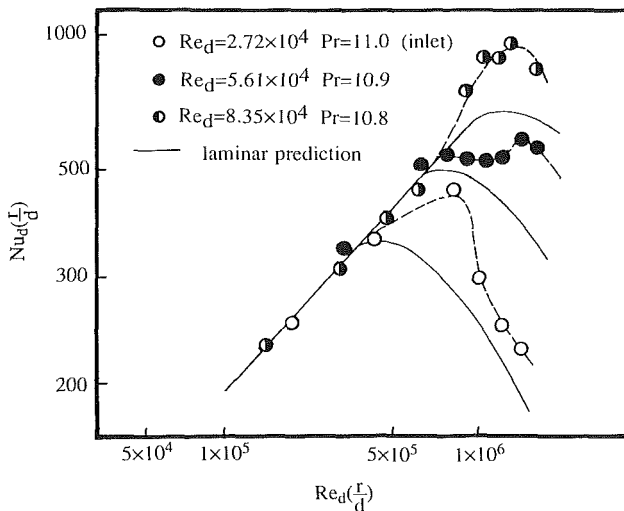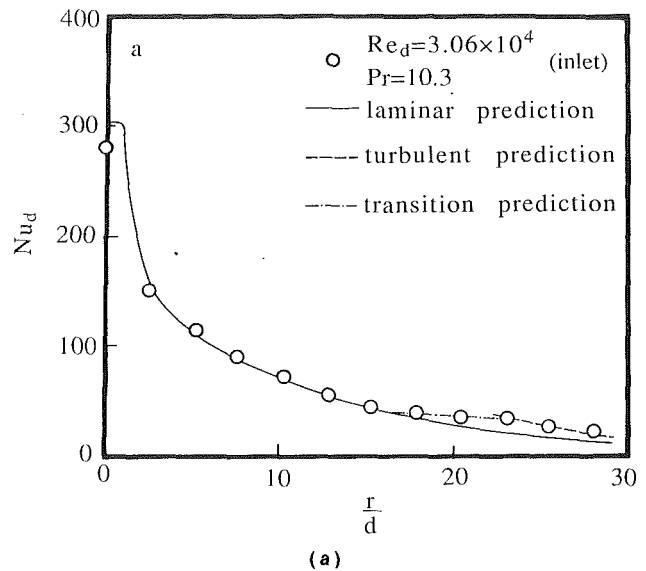**Fig. 11   Measured and predicted Nusselt number in region 2: data for several diameters of orifice**

Fig. 12   Nu$_r$ from data and laminar theory for regions 2 and 3 (— — —: faired curves)

(a)

(b)

Fig. 13   Comparison of data to the laminar and turbulent predictions (predictions follow Table 1)

6(b) shows the simplified integral results, which neglect all terms in ϕ or Δ. In contrast to $Pr > 1$, for $Pr < 1$ the neglected terms are as large as the terms retained when Pr approaches unity. The comparison shows that for $Pr = 0.1$ the disagreement between the integral and differential equations is more than 20 percent. Fortunately, most liquid metals have Pr near 0.01, and for this case the simplified integral results agree with the differential results to better than 5 percent. For larger Prandtl numbers, the higher order terms should be retained when calculating Nu_d.

From the integral analysis, we previously found that the thermal boundary layer would not reach the free surface for $Pr > 5.2$. Therefore, for $Pr > 5.2$, the free surface temperature remains at T_f for all r according to the integral analysis. Of course, this is an approximation based on the assumption of a sharply defined boundary layer. Figure 7 shows the dimensionless free surface temperature from the differential equation solution as function of r/r_0 and illustrates the strong influence of the Prandtl number. For $Pr = 2$, the surface temperature is more than 11 times higher than for $Pr = 10$. For $Pr > 5.2$, the free surface temperature increases much more slowly. However, the surface temperature does rise above the inlet value for $Pr > 5.2$, and this is another cause of differences between integral and differential solutions for Nu_d.

For engineering purposes, it is convenient to construct a simplified version of the integral or differential predictions. First, we note that, in the Prandtl number range between 1 and 5.2 (for which region 4 is possible), the difference between the integral solutions for region 3 and region 4, if applied at the same Reynolds number and radius, amounts to less than 3 percent. Thus, the equation derived for region 3 can usually be applied as a good approximation in region 4 as well.

For futher simplification, we may consider $r/d \gg 0.322$ $Re^{1/3}$ and neglect the terms in d/r and C_3 in the integral result for region 3 (equation (3)):

$$Nu_d = 0.172\, Re_d\, Pr^{1/3} \left(\frac{d}{r}\right)^2 \qquad (34)$$

Correlation of the differential equation solutions (accurate to ± 9 percent) leads to the following, similar result for $1 < Pr < 100$ and $2.5 < r/r_0 < 100$:

$$Nu_d = 0.195\, Re_d^{0.98}\, Pr^{0.38} \left(\frac{d}{r}\right)^{1.95} \qquad (35)$$

For the range $2.5 < r/r_0 < 10$, a slightly better fit (to ± 5 percent) is

$$\mathrm{Nu}_d = 0.15 \, \mathrm{Re}_d^{0.93} \, \mathrm{Pr}^{0.38} \left(\frac{d}{r}\right)^{1.80} \tag{36}$$

Since a turbulent transition and a hydraulic jump usually occur downstream, the latter equation is more useful. However, neither correlation is reliably accurate in the range $1 \le r/r_0 \le 2.5$; this range is important in practice, and we recommend use of the theoretical prediction, equation (3), in region 3. The integral prediction for region 2 is equation (2). For laminar flow, equations (2) and (3) can be used to estimate the local Nusselt number. These predictions are compared with our experimental data below.

The preceding results do not mean that the identification of regions 3 and 4 is unimportant. In region 4, liquid surface temperature increases rapidly with radius, and evaporation can become very significant. Conversely, in region 3, evaporation can be less important for low initial liquid temperature. Thus, for lower Prandtl numbers, the surface temperature should always be estimated, and, if necessary, the adiabatic surface condition should be dropped in favor of an evaporating surface condition. Surface evaporation was carefully suppressed in the present experiments by cooling the incoming liquid and by limiting the heat flux, but in engineering applications, evaporation will almost always occur. Evaporation will tend to raise Nu_d (Liu and Lienhard, 1989), since it offers an additional heat sink, unless it leads to film dryout downstream, in which case Nu_d will drop disastrously.

The numerical solutions with constant Prandtl number suggest Nusselt number is proportional to Prandtl number to the 0.38 power over Prandtl number from 1 to 100. However, most liquids of high Prandtl number show a rapid decrease in Prandtl number with increasing temperature. Streamwise variations in Pr, as bulk temperature rises, are certainly important
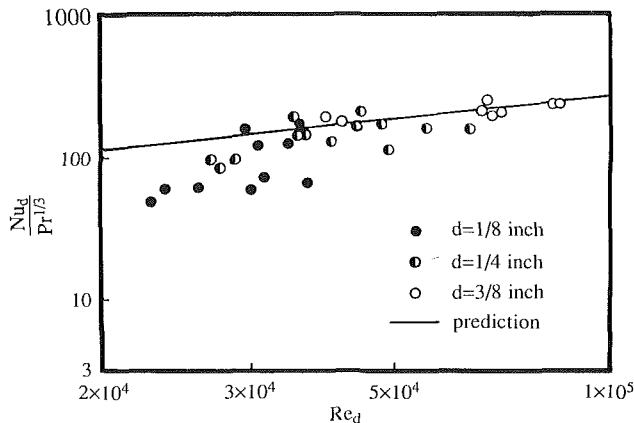

Fig. 14 Measured stagnation point Nusselt number compared to prediction for Pr > 3: data for several diameters of orifice

and probably outweigh any finer adjustments of the Prandtl number exponents. Best agreement with experimental data was obtained when the values of viscosity (i.e., Re_d) and Pr used in the equations were those corresponding to temperatures at the radial midpoint of the film.

4.2 Turbulent Transition. The preceding analyses are based on laminar flow and consider neither surface waves nor turbulent transition. Plainly, it is important to know the location of transition from laminar to turbulent flow. If, in addition, turbulence significantly raises the Nusselt number above the laminar prediction, a separate analysis of the turbulent transport is necessary.

Figure 8 shows measurements of the turbulent transition radius in the present system. The transition point is easily identified, since the laminar liquid sheet is smooth and transparent, while the turbulent liquid sheet has a rough surface, which reflects light and appears bright. The associated surface waves are described by Azuma and Hoshino (1984a) as "lattice-shaped" waves. A curve fit of our data (Gabour, 1991) gives the transition radius as

$$\left(\frac{r_t}{d}\right) \mathrm{Re}_d^{0.422} = 1.2 \times 10^3 \tag{37}$$

In their own system, Azuma and Hoshino measured

$$\left(\frac{r_t}{d}\right) \mathrm{Re}_d^{0.315} = 0.73 \times 10^3 \tag{38}$$

which shows a slightly weaker dependence on Reynolds number, but turbulent transition points normally depend on the disturbances present in a specific system. Equation (37) suggests a coordinate of $(r/d) \, \mathrm{Re}_d^{0.422}$. Using this coordinate, some of the present heat transfer data are shown in Fig. 9. At the transition point, the figure shows a clear shift in the slope of the Nusselt number, which becomes more pronounced at higher Reynolds number. The Nusselt number increases above the laminar trend, as direct comparisons (below) illustrate. Note that the abscissa here is chosen to illustrate the turbulent transition, not the functional dependence of Nu_d on Re_d and Pr; thus, the curves do not collapse to a single line. Moreover, the streamwise changes in the Re_d and Pr dependencies make it impossible to present all of our data, for many different conditions, on a single graph. In this and following figures, we present enough data to illustrate the general behavior without attempting to be exhaustive.

The Nusselt numbers show a hump downstream of the turbulent transition point. This hump corresponds to the point at which the turbulence has become fully developed (see heat transfer predictions below). As the Reynolds number increases, the hump becomes more pronounced and occurs after shorter distance. The transition and hump radii are shown as a function of jet Reynolds number in Fig. 10. The data for the hump position can be correlated as

Table 1   Suggested formulae for local Nusselt number for Pr ≥ $O(1)$

Region	Range	Nu_d
Stagnation zone	$0 \le r/d < 0.787, \quad 0.15 \le \mathrm{Pr} \le 3$ $\mathrm{Pr} > 3$	$0.715 \, \mathrm{Re}_d^{1/2} \mathrm{Pr}^{0.4}$ $0.797 \, \mathrm{Re}_d^{1/2} \mathrm{Pr}^{1/3}$
Transition: stagn. to b.l.	$0.787 < r/d < 2.23$	$\left(\dfrac{\frac{27}{80} \mathrm{Re}_d \mathrm{Pr} \frac{r}{d}}{\frac{1}{2}\left(\frac{r}{d}\right)^2 - 0.2535} \right)^{1/3}$
b.l. region (2)	$2.23 < r/d < 0.1773 \, \mathrm{Re}_d^{1/3}$	$0.632 \, \mathrm{Re}_d^{1/2} \mathrm{Pr}^{1/3} \left(\frac{d}{r}\right)^{1/2}$
Similarity region (3 & 4)	$0.1773 \, \mathrm{Re}_d^{1/3} < r/d < 1200 \, \mathrm{Re}_d^{-0.422}$ $(r_0/d < r/d < r_t/d)$	$\dfrac{0.407 \, \mathrm{Re}_d^{1/3} \mathrm{Pr}^{1/3} \left(\frac{d}{r}\right)^{2/3}}{\left[0.1713\left(\frac{d}{r}\right)^2 + \frac{5.147 r}{\mathrm{Re}_d d} \right]^{2/3} \left[\frac{1}{2}\left(\frac{r}{d}\right)^2 + C_3 \right]^{1/3}}$ $\left(C_3 = \dfrac{0.267 (d/r_0)^{1/2}}{\left[0.1713\left(\frac{d}{r_0}\right)^2 + \frac{5.147 r_0}{\mathrm{Re}_d d} \right]} - \frac{1}{2}\left(\frac{r_0}{d}\right)^2 \right)$
Transition: laminar/turb.	$1200 \, \mathrm{Re}_d^{-0.422} < r/d < 2.86 \times 10^4 \, \mathrm{Re}_d^{-0.68}$	$\mathrm{Nu}_{lam}(r_t) + [\mathrm{Nu}_{turb}(r_h) - \mathrm{Nu}_{lam}(r_t)]\frac{(r - r_t)}{(r_h - r_t)}$
Turbulent region	$r/d > 2.86 \times 10^4 \, \mathrm{Re}_d^{-0.68}$	$\dfrac{8 \, \mathrm{Re}_d \mathrm{Pr} f(C_f, \mathrm{Pr})}{49(h/r)(r/d) + 28(r/d)^2 f(C_f, \mathrm{Pr})}$

$$\left(\frac{r_h}{d}\right)\mathrm{Re}_d^{0.68}=2.86\times10^4 \tag{39}$$

Recall that the border of region 2 is $r_0/d = 0.1773\mathrm{Re}_d^{1/3}$. This implies that if $\mathrm{Re}_d > 1.1 \times 10^5$, the transition will take place in region 2. For the present Reynolds number range, transition always occurs in the similarity region (region 3). Indeed, the stability analysis of Azuma and Hoshino (1984d) suggests that the flow will always be most unstable near the border of regions 2 and 3, with waves or turbulence commencing in the similarity region.

Figure 11 shows a comparison of the data to the integral solution (equation (2)) in region 2. The agreement is generally within the uncertainty of the data. This region is relatively small. In this region, small concentric ripples can be observed (called "disturbance" waves by Azuma and Hoshino). These waves do not develop significantly, and they appear to have no strong effect on the heat transfer.

In the similarity region, our heat transfer data show a clear transition from laminar to turbulent flow. Azuma and Hoshino (1984a) report a critical (transition) discharge Reynolds number, based on the jet diameter, of 4.8×10^4. From our data this critical discharge Reynolds number is much lower (less than 2×10^4). This discrepancy may be caused by the definition of the critical discharge Reynolds number adopted by Azuma and Hoshino. They regarded the flow to be turbulent when the so-called "sandpaperlike" waves are present over 50 percent of the azimuthal direction, and took that discharge Reynolds number as the critical value. That type of situation never occurs in the present experiments; here with increasing Reynolds number, waves and disturbances inside the liquid sheet intensify, but the transition circle stays essentially circular and symmetric at all Re_d.

The laminar analysis predicts that for a given Re_d, $\mathrm{Nu}_r = (r/d)\,\mathrm{Nu}_d$ reaches a peak value and then decreases. Figure 12, however, shows two features that differ from the prediction. The first is that the data break from the initially linear portion of the laminar prediction at a higher value of Nu_r than predicted. The other is a sharp peak in Nu_r downstream of the change in slope. The first feature suggests, from our observations and those of Azuma and Hoshino's (1984a, 1984d), that the disturbance waves have intensified in this portion of the film. They appear to increase the heat transfer coefficients by up to 20 percent in this short region, which is just ahead of the transition radius where sandpaperlike waves occur (see also Fig. 13b). The second feature, the peak, is simply the hump at full development of turbulence, as previously discussed.

The friction coefficient measurements and mass transfer data of Nakoryakov et al. show a very similar behavior. The primary difference is that turbulent transition, as deduced from their friction coefficient measurements, occurs in the boundary layer region (region 2). Their data show a single peak rather than the pair of features seen here. This suggests that the sheet has become turbulent before surface waves can contribute significantly to the heat transfer. They attribute the peak to waves rather than turbulent transition. However, for their Reynolds number range, the turbulent transition is a more likely explanation.

4.3 Prediction of Turbulent Heat Transfer. The Nusselt number turbulent flow may be calculated using the thermal law of the wall. The Stanton number is defined as

$$\mathrm{St}=\frac{q_w}{\rho c_p u_{\max}(T_w-T_{sf})} \tag{40}$$

and the law of the wall may be written in the standard internal-flow form

$$\mathrm{St}=\frac{C_f/2}{1.07+12.7(\mathrm{Pr}^{2/3}-1)\sqrt{C_f/2}}=f(C_f,\mathrm{Pr}) \tag{41}$$

The skin friction coefficient is calculated from the Blasius law

$$C_f=0.045\left(\frac{\nu}{u_{\max}h}\right)^{1/4}=0.073\mathrm{Re}_d^{-1/4}\left(\frac{r}{d}\right)^{1/4} \tag{42}$$

where the 1/7 power turbulent velocity distribution produces a maximum velocity

$$u_{\max}=\frac{1}{7}\frac{u_f d^2}{hr} \tag{43}$$

and a film thickness h of

$$h=d\left(\frac{0.02091}{\mathrm{Re}_d^{1/4}}\left(\frac{r}{d}\right)^{5/4}+C\frac{d}{r}\right) \tag{44}$$

with

$$C=0.1713+\frac{5.147}{\mathrm{Re}_d}\frac{r_t}{d}-\frac{0.02091}{\mathrm{Re}_d^{1/4}}\left(\frac{r_t}{d}\right)^{1/4} \tag{45}$$

From the above, the Nusselt number for turbulent flow may be calculated:

$$\mathrm{Nu}_d=\frac{8\mathrm{Re}_d\mathrm{Pr}f(C_f,\mathrm{Pr})}{49\left(\frac{h}{r}\right)\left(\frac{r}{d}\right)+28\left(\frac{r}{d}\right)^2 f(C_f,\mathrm{Pr})} \tag{46}$$

When $\mathrm{Pr} \gg 1$, the equation simplifies to

$$\mathrm{Nu}_d=0.0052\mathrm{Re}_d^{3/4}\left(\frac{d}{h}\right)\left(\frac{d}{r}\right)^{3/4}\left(\frac{\mathrm{Pr}}{1.07+12.7(\mathrm{Pr}^{2/3}-1)\sqrt{C_f/2}}\right) \tag{47}$$

The turbulent Nusselt number is substantially higher than the laminar Nu_d.

Figures 13(a, b) show the laminar and turbulent predictions together with experimental data for two runs at different Reynolds numbers. In both cases, agreement is excellent. The increasing strength of turbulent augmentation with increasing Reynolds number is also quite apparent. The only significant disagreement observed is in the stagnation zone for lower Reynolds number. Data and predictions for the stagnation zone are discussed in the next section.

4.4 Stagnation Zone Heat Transfer. In the stagnation zone of a body passing through an infinite fluid medium, White (1974) finds

$$\mathrm{Nu}_d=G(\mathrm{Pr},3)\left(\frac{Bd^2}{\nu}\right)^{1/2} \tag{48}$$

where

$$G(\mathrm{Pr},3)=\begin{cases}0.53898\mathrm{Pr}^{0.4} & 0.15\le\mathrm{Pr}\le3.0\\0.6010\mathrm{Pr}^{1/3}-0.05085 & \mathrm{Pr}\ge3.0\end{cases}$$

The value of $B = 2\partial u/\partial r$ at the stagnation point of an inviscid impinging liquid jet was calculated approximately by Schach (1935)[6]

$$B=1.76\frac{u_f}{d} \tag{49}$$

This value should be applicable for reasonably large jet Reynolds numbers.

From these results

$$\mathrm{Nu}_d=\begin{cases}0.715\,\mathrm{Re}_d^{1/2}\mathrm{Pr}^{0.4} & 0.15\le\mathrm{Pr}\le3\\0.797\,\mathrm{Re}_d^{1/2}\mathrm{Pr}^{1/3} & \mathrm{Pr}>3\end{cases} \tag{50}$$

Figure 14 compares the data to the above equations, illustrating generally good agreement. The data appear to fall below the

---

[6]Schach's Figs. 9 and 10 are a bit garbled. This often-quoted value is obtained from his $\partial v/\partial z$ and continuity.

prediction at lower Reynolds numbers. This behavior may be related to a decrease in the stagnation zone velocity gradient owing to viscous effects, but further study is required.

Nakoryakov et al. (1978) measured the Nusselt number for mass transfer beneath an impinging jet at high Schmidt number with uniform wall concentration. They did not directly test a relation for the stagnation zone transport. Instead, they used a relation for Nu (equation (1)) to calculate their jet velocities. The relation they used seems to be quite close to that suggested above, although its origin remains obscure (it does not appear in the reference they cite). Nakoryakov et al. also measured wall shear stress in the stagnation zone, but the calibration of their stress probe was similarly based on an assumed value of $\partial u / \partial r$.

Stevens and Webb (1989) used a pipe-type nozzle producing turbulent incoming jets, and their measured Nusselt numbers are in the same general range, although a bit higher, than the present data. They represented their stagnation zone results by a correlation that accounts for the Reynolds number dependence of the stagnation velocity gradient with a dimensional correlating factor of u_f/d

$$\mathrm{Nu}_d = 2.67 \mathrm{Re}_d^{0.57} \left(\frac{z}{d}\right)^{-1/30} \left(\frac{u_f}{d}\right)^{-1/4} \mathrm{Pr}^{0.4} \qquad (51)$$

where z is the distance of their nozzle from the heater. This correlation shows a somewhat different dependence on jet diameter and velocity than is found for the present laminar jets. Stevens and Webb present a second correlation for the radial variation Nu_d, which does not represent the present data well at the large radii of interest to us, although it does represent their own data very well for r/d less than about 5.

The size of the stagnation zone may be estimated by calculating the radius at which the stagnation boundary layer and the region 2 boundary layer have the same thickness (i.e., $2.107 \, d \, \mathrm{Re}_d^{1/2} = 2.679 \, (rd/\mathrm{Re}_d)^{1/2}$; White, 1974; Sharan, 1984). The result is

$$\frac{r_m}{d} = 0.787 \qquad (52)$$

Similarly, Stevens and Webb found the stagnation region beneath a turbulent jet to reach to roughly $r/d = 0.75$. Our crude estimate shows that the stagnation zone is very small. Its primary importance is that it possesses the maximum local heat transfer coefficient (lowest wall temperature) in the flow. It contributes little, however, to overall heat removal or downstream Nusselt numbers as may be seen from the full integral result for region 2 (Liu and Lienhard, 1989), which does not neglect the stagnation zone heat flow as does equation (2):

$$\mathrm{Nu}_d = \left(\frac{\frac{27}{80} \mathrm{Re}_d \mathrm{Pr} \frac{r}{\delta}}{\frac{1}{2} \left(\frac{r}{d}\right)^2 + C_2} \right)^{1/3} \qquad (53)$$

with $\delta = 2.679 \, (rd/\mathrm{Re}_d)^{1/2}$. At $r = r_m$, the Nusselt number should equal the stagnation zone Nusselt number; thus,

$$C_2 = -0.2535 \qquad (54)$$

The error in Nu_d caused by neglecting the stagnation zone is less than 10 percent for $r/d > 2.23$.

4.5 Recommendations for Nusselt Number Estimation. Table 1 summarizes the suggested relations for estimating local Nusselt number for impinging, circular, free liquid jets. For most regions, deviations are less than 10 percent. For laminar convection in the similarity region, however, waves can enhance the heat transfer, and Nu_d may exceed the estimate by up to 20 percent; as the waves are damped, the heat transfer goes back down. The wavy region is relatively small, however, because it is limited by subsequent turbulent transition. In the region of transition from laminar to turbulent flow, between

r_t and r_h, we tentatively recommend a line fit between the laminar predictions at r_t and the turbulent prediction at r_h. This fit is shown in Figs. 13 (a, b) and can be seen not to account properly for the wave effects that occur in that region at larger Reynolds number. With the exceptions of this line fit and the correlation for r_t/d, all equations in Table 1 are analytical predictions; each is substantiated by experiment.

4.6 Additional Studies Required. In jet impingement cooling applications, turbulent incoming jets are likely to be produced, since upstream disturbances are not usually damped and the jets often issue from pipes. While turbulence may enhance stagnation point heat transfer, it is damped sharply as the film spreads. We are currently conducting experimental studies of turbulent jet heat transfer.

Impinging jets will splatter if the jet surface is even slightly disturbed or the thin liquid sheet is disturbed beyond a certain magnitude. Disturbances to the incoming jet are often caused by irregularities in the orifice or by turbulence in the liquid supply. Roughness of the target surface can also disturb the liquid film. Splattering removes liquid from the liquid film, and thus lowers the Nusselt number; Liu and Lienhard (1989) estimated reductions of 20 percent or more. We are also investigating the role of splattering in jet impingement cooling.

Finally, the behavior of the stagnation zone at lower Reynolds number will be further investigated, owing to surface tension effects and a possible viscous decrease of the stagnation velocity gradient as Re_d becomes smaller.

Conclusions

Convective heat removal by liquid jet impingement has been investigated for uniform wall flux and circular, laminar jets. Both theoretical and experimental results are given.

- The radial distribution of Nusselt number is accurately predicted by the formulae in Table 1 for Prandtl numbers of order unity or greater.
- Laminar heat transfer in the film for $\mathrm{Pr} \geq O(1)$ may be calculated from equation (2) in the boundary layer region (region 2) and by equation (3) in the laminar portion of the similarity region (regions 3 and/or 4). These regions are described in Section 2.1.
- Laminar heat transfer predictions for $\mathrm{Pr} < 1$ are developed in Section 2.2.
- Comparison of the integral predictions to numerical solutions in the similarity region supports conclusions previously drawn from the integral approach for $\mathrm{Pr} > 1$ as well as the new results for $\mathrm{Pr} < 1$.
- Turbulent transition occurs at a radius given by equation (37). Turbulence becomes fully developed at a radius given by equation (39). Turbulent heat transfer in the film is given by equation (46).
- The stagnation point Nusselt number is reasonably well represented by equation (50).

Acknowledgments

References

Azuma, T., and Hoshino, T., 1984a, "The Radial Flow of a Thin Liquid Film, Part 1: Laminar–Turbulent Transition," *Trans. Japan Soc. Mech. Engrs.*, Vol. 50, p. 974.

Azuma, T., and Hoshino, T., 1984b, "The Radial Flow of a Thin Liquid Film, Part 2: Film Thickness," *Trans. Japan Soc. Mech. Engrs.*, Vol. 50, p. 902.

Azuma, T., and Hoshino, T., 1984c, "The Radial Flow of Thin Liquid Film, Part 3: Velocity Profile," *Trans. Japan Soc. Mech. Engrs.*, Vol. 50, p. 1126.

Azuma, T., and Hoshino, T., 1984d, "The Radial Flow of Thin Liquid Film, Part 4: Stability of Liquid Film and Wall Pressure Fluctuation," *Trans. Japan Soc. Mech. Engrs.*, Vol. 50, p. 1136.

Carper, H. J., 1989, "Impingement Cooling by Liquid Jet," presented at the ASME Winter Annual Meeting, San Francisco, CA.

Chaudhury, Z. H., 1964, "Heat Transfer in a Radial Liquid Jet," *J. Fluid Mech.*, Vol. 20, pp. 501–511.

Errico, M., 1986, "A Study of the Interaction of Liquid Jets With Solid Surfaces," Doctoral Thesis, University of California at San Diego.

Gabour, L. A., 1991, "Heat Transfer to Turbulent and Splattering Impinging Liquid Jets," S. B. Thesis in Mechanical Engineering, MIT, Cambridge, MA.

Ishigai, S., Nakanishi, S., Mizuno, M., and Imamura, T., 1977, "Heat Transfer of the Impinging Round Water in the Interference Zone of Film Flow Along the Wall," *Bulletin of the JSME*, Vol. 20, No. 139.

Liu, X., and Lienhard V, J. H., 1989, "Liquid Jet Impingement Heat Transfer on a Uniform Flux Surface," *Heat Transfer Phenomena in Radiation, Combustion, and Fires,* ASME HTD-Vol. 6, pp. 523–530.

Lombara, J. S., 1990, "An Experimental Investigation of Liquid Jet Impingement Heat Transfer Theories," S. B. Thesis in Mechanical Engineering, MIT, Cambridge, MA.

Nakoryakov, V. E., Pokusaev, B. G., and Troyan, E. N., 1978, "Impingement of an Axisymmetric Liquid Jet on a Barrier," *Int. J. Heat Mass Transfer*, Vol. 21, pp. 1175–1184.

Olsson, R. G., and Turkdogan, E. T., 1966, "Radial Spread of a Liquid Stream on a Horizontal Plate," *Nature*, Vol. 211, No. 5051, pp. 813–816.

Schach, W., 1935, "Umlenkung eines kreisförmigen Flussigkeitsstrahles an einer ebenen Platte senkrecht zur Strömungsrichtung," *Ing.-Arch.*, Vol. 6, pp. 51–59.

Schlichting, H., 1979, *Boundary-Layer Theory*, 7th ed., McGraw-Hill, New York.

Sharan, A., 1984, "Jet-Disc Boiling: Burnout Predictions and Application to Solar Receivers," Master's Thesis in Mechanical Engineering, University of Houston, TX.

Stevens, J., and Webb, B. W., 1989, "Local Heat Transfer Coefficients Under an Axisymmetric, Single-Phase Liquid Jet," *Heat Transfer in Electronics—1989,* ASME HTD-Vol. 111, pp. 113–119.

Vasista, V. K., 1989, "Experimental Study of the Hydrodynamics of an Impinging Liquid Jet," Bachelor's Thesis in Mechanical Engineering, MIT, Cambridge, MA.

Wang, X. S., Dagan, Z., and Jiji, L. M., 1989a, "Heat Transfer Between a Circular Free Impinging Jet and a Solid Surface With Nonuniform Wall Temperature or Wall Heat Flux—1. Solution for the Stagnation Region," *Int. J. Heat Mass Transfer*, Vol. 32, No. 7, pp. 1351–1360.

Wang, X. S., Dagan, Z., and Jiji, L. M., 1989b, "Heat Transfer Between a Circular Free Impinging Jet and a Solid Surface With Nonuniform Wall Temperature or Wall Heat Flux—2. Solution for the Boundary Layer Region," *Int. J. Heat Mass Transfer*, Vol. 32, No. 7, pp. 1361–1371.

Wang, X. S., Dagan, Z., and Jiji, L. M., 1989c, "Conjugate Heat Transfer Between a Laminar Impinging Liquid Jet and a Solid Disk," *Int. J. Heat Mass Transfer*, Vol. 32, No. 11, pp. 2189–2197.

Watson, E. J., 1964, "The Radial Spread of a Liquid Over a Horizontal Plane," *J. Fluid Mech.*, Vol. 20, pp. 481–499.

White, F. M., 1974, *Viscous Fluid Flow*, McGraw-Hill, New York.

CORRECTIONS OF LAMINAR IMPINGING JET EQUATIONS

J.H. LIENHARD V

The equation for C_3 is a bit complicated, and it has repeatedly carried typographical errors of one sort or another. These errors appear in: Liu and Lienhard (1989, eq. 16); Liu, Lienhard and Lombara (1991, eq. 4); Lienhard (1995, Table 5); and Lienhard (2006, eq. 36).

The correct equation for C_3 is:

$$ (1) \qquad C_3 = \frac{0.267(d/r_0)^{1/2}}{\left[0.1713\,(d/r_0)^2 + (5.147\,r_0/\mathrm{Re}_d\,d)\right]^2 \mathrm{Re}_d^{1/2}} - \frac{1}{2}\left(\frac{r_0}{d}\right)^2 $$

Equation (78) and Table 5 in Lienhard (1995) give an incorrect expression for Nu_d. The correct expression is:

$$ (2) \qquad \mathrm{Nu}_d = \frac{q_w\,d}{k(T_w - T_f)} = \frac{8\,\mathrm{Re}_d\mathrm{Pr}\,f(C_f,\mathrm{Pr})}{49\,(hr/d^2) + 28\,(r/d)^2\,f(C_f,\mathrm{Pr})} $$

REFERENCES

[1] X. Liu and J.H. Lienhard V, 1989, "Liquid Jet Impingement Heat Transfer on Uniform Heat Flux Surface," *Heat Transfer Phenomena in Radiation, Combustion, and Fires*, ASME HTD, Vol.106, pp.523-530. (26th ASME/AIChE National Heat Transfer Conference, Philadelphia, Aug. 6-9, 1989)

[2] X. Liu, J.H. Lienhard V, and J.S. Lombara, 1991, "Convective Heat Transfer by Impingement of Circular Liquid Jets," *J. Heat Transfer,* Vol. 113, No. 3, pp. 571-582.

[3] J.H. Lienhard V, 1995, "Liquid Jet Impingement," *Annual Review of Heat Transfer,* C.L. Tien ed., Vol. 6, Chpt. 4. New York: Begell House, pp. 199-270.

[4] J.H. Lienhard V, 2006, "Heat Transfer by Impingement of Circular Free-surface Liquid Jets," in S.C. Mishra, B.V.S.S.S. Prasad, and S.V. Garimella (eds.), *Heat and Mass Transfer 2006*. New Delhi: Tata McGraw-Hill, pp. 211–226. (Proc. 18th Natl. and 7th Intl. ISHMT-ASME Heat and Mass Transfer Conf., Guwahati, India 4–6 Jan. 2006).